Anisotropic Etching of Pyramidal Silica Reliefs with Metal Masks and Hydrofluoric Acid

Robert Kirchner,* Volker Neumann, Felix Winkler, Carsten Strobel, Sandra Völkel, André Hiess, Dimitrios Kazazis, Ulrich Künzelmann, and Johann Wolfgang Bartha

This work describes the fabrication of anisotropically etched, faceted pyramidal structures in amorphous layers of silicon dioxide or glass. Anisotropic and crystal-oriented etching of silicon is well known. Anisotropic etching behavior in completely amorphous layers of silicon dioxide in combination with purely isotropic hydrofluoric acid as etchant is an unexpected phenomenon. The work presents practical exploitations of this new process for self-perfecting pyramidal structures. It can be used for textured silica or glass surfaces. The reason for the observed anisotropy, leading to enhanced lateral etch rates, is the presence of thin metal layers. The lateral etch rate under the metal significantly exceeds the vertical etch rate of the non-metallized area by a factor of about 6–43 for liquid and 59 for vapor-based processes. The ratio between lateral and vertical etch rate, thus the sidewall inclination, can be controlled by etchant concentration and selected metal. The described process allows for direct fabrication of shallow angle pyramids, which for example can enhance the coupling efficiency of light emitting diodes or solar cells, can be exploited for producing dedicated silicon dioxide atomic force microscopy tips with a radius in the 50 nm range, or can potentially be used for surface plasmonics.

The fabrication of inverted pyramidal structures in crystalline silicon is a well-known process based on significantly varying etching rates of different crystal planes.[1,2] Exploiting corner selective masking processes, even 3D fractal crystals can be etched into silicon exploiting crystal-oriented etching.[3] In case of silicon, isotropic etchants such as potassium hydroxide (KOH) or tetramethylammonium hydroxide yield anisotropic structures due to anisotropic material properties (here: etch rates). The slow etch rate of silicon {111} planes enables

the fabrication of inverted silicon pyramids for various applications, e.g., for atomic force microcopy (AFM) tip fabrication, photovoltaics, or infrared spectroscopy.[4–6] Adding surfactants to KOH allows for changing the typical wet etch taper.[7] Metal films have been used for highly selective etching of diamond.[8] Our work on silica surfaces has potential in capillary stamping, plasmonics, photovoltaics, and light emitting diodes.[9–12] So far, amorphous silicon dioxide has not been known to show anisotropic etching behavior in hydrofluoric acid (HF). Usually, isotropic structures, e.g., for microfluidics are obtained.[13] Kometani et al. observed etch enhancement in vapor phase HF etching using titanium and aluminum patterns on silicon dioxide.[14–16] Recently, fast etching of sacrificial Ti layers was utilized to tune sidewall angles in silicon dioxide—a first report on interfacial etching as root cause for similar observations as in this work.[17] It is well accepted that the HF etch rate is substantially influenced by density and composition of oxides.[17] In general, depending on the grade of anisotropy (i.e., the relation of lateral r_l to vertical r_v etch rate) different etch profiles can be obtained (**Figure 1**).

This study demonstrated that anisotropic etch behavior, using certain metals for masking, can be achieved and exploited to create ultra-sharp pyramidal edges starting from convex masking corners. The effect is self-perfecting. As will be shown, a convex corner with a finite fillet radius is transformed into a sharp edge with strongly reduced concave fillet radius. Thus, under square shaped metal masking features perfectly shaped square pyramidal structures are obtained that differ from previously published results.[17] In contrast to isotropic wet etching, the profile of the etch front is not semi-circular (cf. Figure 1a) but linear (cf. Figure 1c). To achieve comparable patterns, high-resolution grayscale lithography along with sophisticated pattern transfer would be required.[18–20,21]

Of course, different shapes of initial patterns are conceivable but this work concentrates on rectilinear shapes (Figure S1, Supporting Information) to obtain pyramidal structures with rectilinear base. The respective metal patterns are obtained via lift-off processing of electron beam evaporated thin gold, platinum, or chromium films with and without titanium adhesion layers. Anisotropic, strongly under-cut metal pads were obtained via HF etching. Various aqueous HF concentrations

Dr. R. Kirchner, Dr. V. Neumann, F. Winkler, Dr. C. Strobel, S. Völkel,
A. Hiess, Dr. U. Künzelmann, Prof. J. W. Bartha
Institute of Semiconductors and Microsystems
Technische Universität Dresden
Dresden 01062, Germany
E-mail: robert.kirchner@tu-dresden.de
Dr. D. Kazazis
Paul Scherrer Institute
Laboratory for Micro- and Nanotechnology
Villigen PSI 5232, Switzerland

The ORCID identification number(s) for the author(s) of this article can be found under https://doi.org/10.1002/smll.202002290.

ADVANCED
SCIENCE NEWS
www.advancedsciencenews.com

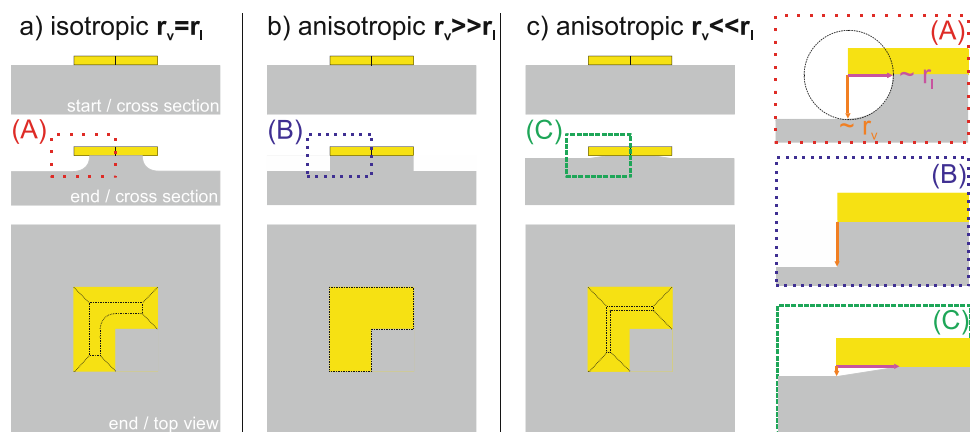NANO · MICRO
small
www.small-journal.com

Figure 1. Schematic for sidewall formation under different etching conditions with different views and zoom-in details: a) isotropic etching (e.g., wet etching) leading to a semicircular profile (detail A), b) completely anisotropic etching with insignificant lateral etch rate (e.g., dry plasma etching) resulting in a linear vertical profile (detail B), and c) strongly anisotropic etching as exploited in this work yielding linearly sloped profiles (detail C).

and buffer solutions as well as vapor-phase HF (vHF) with water and 2-propanol (isopropyl alcohol, IPA) as co-solvents were tested.

Wet etching proceeded with different etch rates for 1 µm thick silicon dioxide layers on {100} silicon substrates depending on the etchant (**Table 1**).

The buffered oxide etch (BOE) produces shallow, smooth, and sharp pyramids with symmetric profile underneath square metal pads (**Figure 2**). The estimated etch rate of wet thermal oxide in 5:1 BOE is about 1.7 nm s^{-1}.[22] The vertical etch rate in the BOE in this work was found to be similar ([1.8 ± 0.2] nm s^{-1}) across several sites on several samples. However, the lateral etch rate was significantly enhanced by a factor of nine (to about [15.7 ± 0.2] nm s^{-1}). The sidewall inclination was 7° underneath the square metal pad on each side (Figure 2d). This inclination is defined by the ratio of lateral r_l to vertical r_v etch rate. The determined etch rates of 15.7 and 1.8 nm s^{-1} were expected to result in an angle of 6.5°, which coincides well with the value of 7° as measured by AFM in this work and reported in literature by others.[17] The slope of the inclination was constant indicating the existence of a constant etching behavior over time, i.e., without significant delay in the beginning or gradually attenuation/gain during the etching.

An ideally isotropic etch profile has a semi-circular cross section due to constant etch rates in all spatial directions (cf. Figure 1 detail A). The normalized experimentally observed profiles significantly deviated from that (cf. Figure S2, Supporting Information). A substantially enhanced etch rate was mostly present in the direction parallel to the surface (0° angle in Figure S2b, Supporting Information) while approaching unity, i.e., the ideal isotropic behavior for directions normal to the surface (90° angle in Figure S2b, Supporting Information). Clearly, fast etching was obtained in the direction parallel to the surface and along the metal-silicon dioxide interface. This might be caused by differences in oxide density well known to influence etch rates.[23] Another explanation is the presence of a different material such as titanium that will be etched much faster than silicon dioxide. A non-ideal adhesion of the metal mask to the etched substrate was reported to cause enhanced lateral under-etch and a tapered profile.[17] In contradiction, for etch resistant Cr layers without Ti adhesion promoter, still similar etch behavior was observed. Stress can be excluded because it will be rather concentrated in the thin metal film than in the thick SiO$_2$ layer. Due to deposition processes, evaporated films are usually under tensile stress with a stress gradient normal to the surface.[24] As a consequence, all metal sections would bend upward during release etching, and therefore they cannot adhere to or interact with the substrate.

The production of ideal pointy pyramids would require the termination of the etching process at a defined time. The etching process in Figure 2d was stopped before the top-tip was formed (under-etch situation). Over-etching will reduce the total height of the pyramid, but still sharp edges and top-tips will remain (Figure 2c). Differences in pyramidal height across the sample originated from different lateral advancement of the etch front depending on its chronological start and potential over-etching time. Figure 2c and the profile in Figure 2d confirm a complete removal of the oxide layer outside the metal region. The thin evaporated metal film sticks to the silicon substrate due to capillary forces during the drying process.

Although the convex corners of the metal mask are not ideally pointy, the resulting ridge starting from this corner
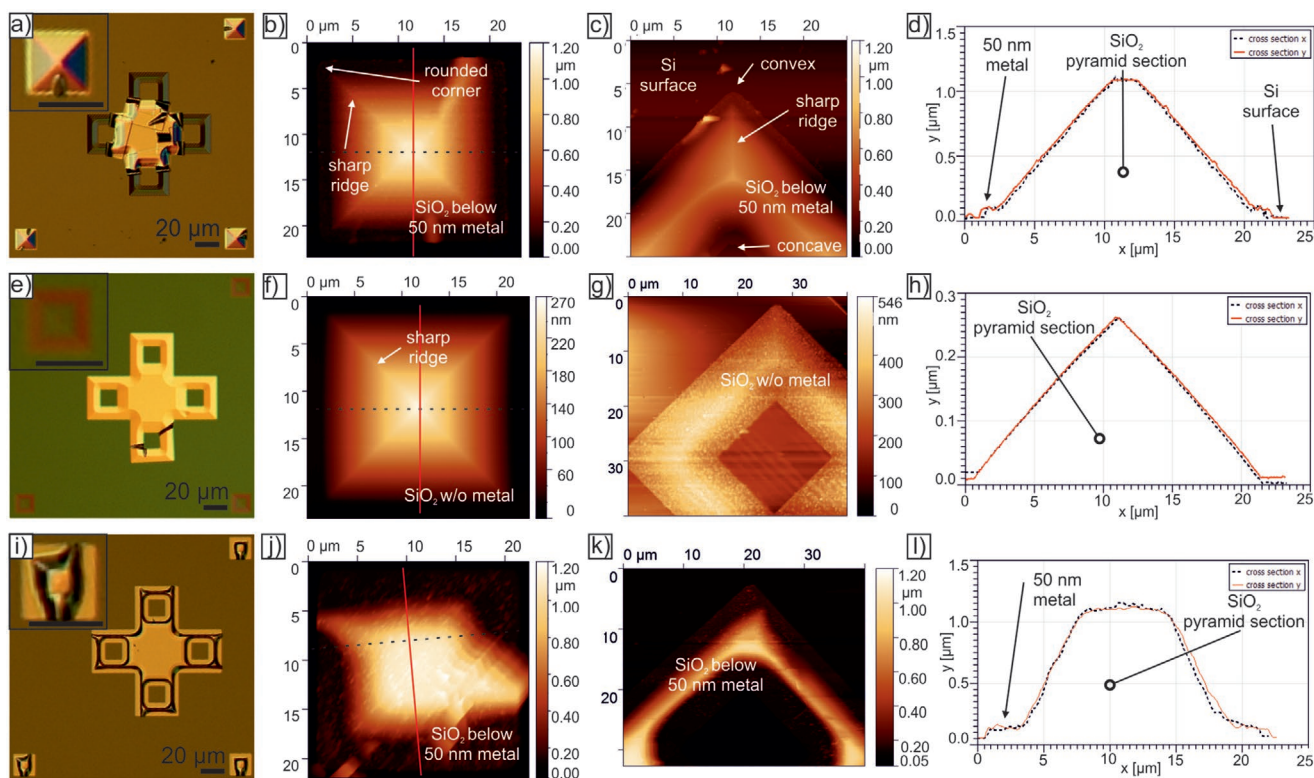
Table 1. Experimentally obtained etch behavior depending on used etch chemistries for wet, and as reference for vapor phase, etching of 1 µm wet thermal SiO$_2$ on {100} silicon substrates with 5 nm Ti/50 nm Au masking. (BOE: buffered oxide etch, HF: hydrofluoric acid, IPA: isopropyl alcohol).

	BOE wet ≈5% HF	5% HF wet Unbuffered	50% HF wet Unbuffered	4:1 50% HF:IPA vapor 40 °C substrate
Vertical rate r_v (nm s^{-1})	1.8	0.4	7.5	0.14 (v)
Lateral rate r_l (nm s^{-1})	15.7	17.2	42.9	8.3 (l)
Inclination *(°)	6.5	1.3	9.7	1.0
Ratio r_l/r_v	8.7	43.0	5.7	59.3

[(v): vapor phase etching, (l): liquid phase etching due to condensation]. *Estimated from ratio r_l/r_v, r_l: lateral etch rate, r_v: vertical etch rate.

**ADVANCED
SCIENCE NEWS**

www.advancedsciencenews.com

NANO · MICRO

small

www.small-journal.com

Figure 2. Topography with and without 5 nm Ti/50 nm Au overlay film after applying different wet etchants: a–d) 10 min BOE etching (with overlay), e–h) 10 min 5% unbuffered HF (without overlay), i–l) 2 min 50% unbuffered HF (with overlay). Optical microscopy (a, e, i), AFM height image of a pattern beneath a square metal pad masked region (b, f, j), AFM height image of the corner region of an open square (c, g, k), and cross section from (b, f, j) along horizontal and vertical direction (d, h, l).

is significantly more pointy (Figure 2b,c). As expected from theory, concave corners had an isotropic and curved etch profile (Figure 2c), whereas convex corners had a sharp anisotropic etch profile (Figure 2c). While the detailed reason for the enhancement of under-etching remains questionable, the following model (**Figure 3**) can explain the observed isotropic in-plane under-etching of convex and concave corners. In convex corners, two etch fronts start from the mask edge and proceed normal to it with the isotropic in-plane etch rate r (Figure 3a). At the intersection of both etch fronts, a sharp
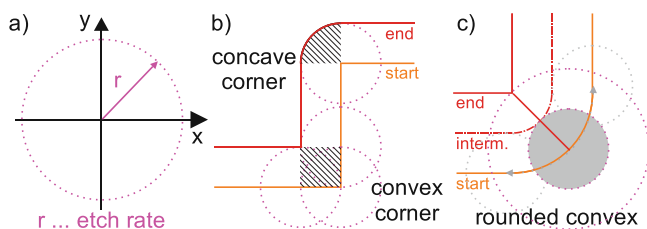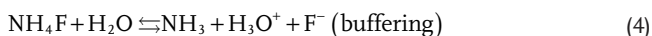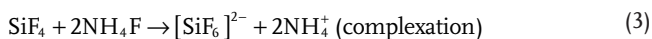
corner is produced (Figure 3b). As observed in the experiment, this process creates over time self-perfecting corners (Figure 3c): the material in the hatched region in Figure 3b of the convex corner is irreversibly lost due to two proceeding fronts moving *"towards each other."* In contrast, the hatched region in concave corners represents material that is newly exposed due to two fronts moving *"apart from each other."* As a consequence, in-plane convex corners become sharp 3D ridges, and concave corners become 3D rounded slopes. The concave corner behavior was also observed by Pekas et al. before.[17]

In general, similar observations were found for etching with 5% (Figure 2e–h) and 50% (Figure 2i–l) unbuffered HF. However, the specific profiles were significantly different due to different etch rate ratios. Unbuffered 5% HF etches by a factor of five slower in the unmasked area (0.4 nm s^{-1}, cf. Table 1) compared to buffered HF mixture of the same HF concentration (1.8 nm s^{-1}, cf. Table 1). In unbuffered HF solutions, there is a consumption of fluoride ions while buffered solutions enhance etching behavior due to additional as well as replenished fluorine species.[23,25] HF etching results always in water formation as reaction byproduct. Both effects—fluoride consumption and water formation—cause a decreased etch rate in unbuffered solutions. In the buffered etchant, fluoride ions are continuously fed back. Even though the etching process might involve different fluoride species, the etching process can be generalized as follows:[23,25]

Figure 3. Schematic situations for moving etch fronts following construction rules for isotropic etching behavior of SiO$_2$: a) constant etch rate r versus spatial angle (hence isotropic), b) ideal concave and convex corners [hatched regions are either irreversibly lost (convex) or newly created (concave)], c) real rounded convex corner [gray arrows: virtually moving the isotropic spatial etch profile along starting geometry explains corner sharpening].

ADVANCED
SCIENCE NEWS
www.advancedsciencenews.com

NANO · MICRO
small
www.small-journal.com

unbuffered oxide etch

$$SiO_2 + 4HF \rightarrow SiF_4 + 2H_2O \tag{1}$$

$$SiO_2 + 6HF \rightarrow H_2SiF_6 + 2H_2O \tag{2}$$

additionally in BOE

$$SiF_4 + 2NH_4F \rightarrow [SiF_6]^{2-} + 2NH_4^+ \text{ (complexation)} \tag{3}$$

$$NH_4F + H_2O \leftrightarrows NH_3 + H_3O^+ + F^- \text{ (buffering)} \tag{4}$$

Despite differences in the unmasked regions, the lateral etch rate under the metal is nearly the same for buffered 5% HF (15.7 nm s^{-1}, cf. Table 1) and unbuffered 5% HF (17.2 nm s^{-1}, cf. Table 1). Consequently, the obtained pyramids are very shallow (1–2° slope) for unbuffered 5% HF. Notably, this indicates different etching kinetics for different regions. In most cases, HF etching is considered to be reaction limited.[17] However, in thin capillaries it is expected to be diffusion limited.[17] Below the metal mask, the chemical reaction with the SiO$_2$ does not seem to be affected by the consumption of fluoride ion species or the production of water as reaction byproduct. Figure 2f demonstrates the fabrication of ideal pyramids with about 50–100 nm tip radius. Obviously, since etching was not specifically terminated, the formation of the pyramid tip must have been self-perfecting (Figure 2h) due to meeting of four etch fronts having moved toward each other. More strikingly, while the feature height in Figure S8c,d (Supporting Information) was 650–700 nm, the height for smaller features at the same sample was only about 550 nm in Figure S7a,b (Supporting Information)—indicating a clear over-etch—but still provided sharp top corners and ridges.

Neither the buffered nor the unbuffered HF etching in situ etch observation (Figure S3, Supporting Information) did indicate any kind of direct physical contact between metal surface and oxide during etching. The sticking of the thin and flexible metal films did not take place until the sample drying. So, any kind of interpretation as mechanically triggered or supported effect can be ruled out. This includes the mechanism of metal-assisted SiO$_2$ etching as it would require a continuous and close contact of the metal to the silicon oxide surface.[22] This could have been the case only for a limited region just before under-etching.

At high HF concentration of 50% (Figure 2i–l), all etch rates increased as expected due to higher concentration of reactive ion species.[22] For all etchants tested, the etch profile is strongly linear. However, the enhancement of the lateral versus the vertical etch is significantly smaller for the 50% HF in comparison to both 5% HF solutions (cf. Table 1). As the etch rate ratio is the smallest, the inclination of the sidewall is the largest for 50% HF.

In conclusion, the low HF concentration yielded by far the most selective etching. Assuming a non-affected oxide, the reaction for the fluoride species should proceed with the same speed independent of the presence of the metal film. Depending on the metal pad geometry, complete or truncated cones with circular bases could also be obtained (Figures S8 and S9, Supporting Information). It is known that temperature can enhance the HF etch rate for different materials. However, the final obtained shape might be constant due to constant ratios of the increased etch rates.[17]
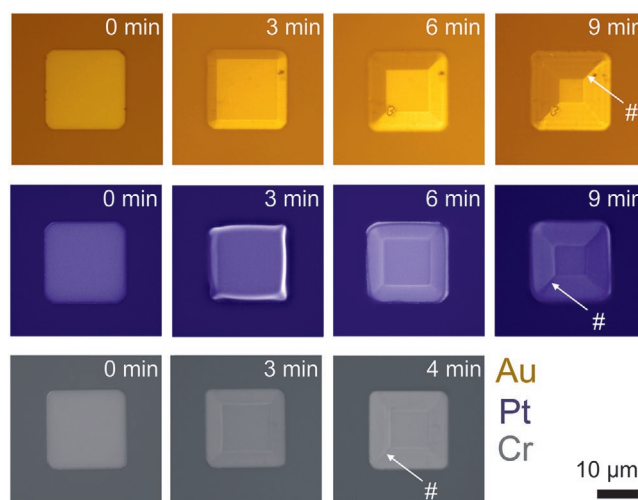

Figure 4. Under-etch behavior of different metal masks (optical microscopy top view after rinsing and drying) indicating different metal behavior as well as confirming before observed corner sharpening and self-perfectioning (denoted by symbol #).

There is another contribution to the etching effect—the used masking material itself (**Figure 4**). All materials were electron beam evaporated without breaking the high vacuum. According to William et al., the etch rate of evaporated Au, Pt, and Cr is below 0.1 nm s^{-1} for 5:1 BOE and 10:1 HF, respectively.[26] In contrast, sputtered Ti is known to be well etched in 5:1 BOE and in 10:1 HF with large etch rates of 18.3 nm s^{-1} being reported.[26] Thus, the Ti adhesion layer etches the fastest, reducing the adhesion of the metal stack to the SiO$_2$ surface and might enhance the lateral under-etch. Surprisingly, this lateral etch rate varied with the used *inert* cover metal Au, Pt, or Cr (Figure 4). Similar etch behavior was even obtained for Cr films *without* Ti adhesion layer. Table 2 summarizes the lateral etch rates for different materials used in this study. While Ti/Au, Ti/Pt, and pure Cr had a comparable under-etch rate, Ti/Cr was faster under-etched by a factor of almost two compared to the other materials. This might be due to the HF-induced intergranular corrosion of metallic Cr.[27]

It is known that metals are able to increase chemical reaction rates catalytically. As an example, Au and Pt act as catalysts for oxygen reduction as one of the reaction steps in metal-assisted etching of silicon.[22] However, at the SiO$_2$ surface, catalytic activity—if there is any—would be limited to the oxide etching reaction. In our experiments very similar oxide etch rates for Au and Pt masking were observed despite their known different catalytic properties.[22] Etching rates were estimated from optical micrographs. Remarkably, Cr as catalytically inactive material (regarding oxygen reduction) yields the highest etching rate in combination with Ti adhesion layer being about 1.8 times faster than Au and Pt. In conclusion, catalytic activity can be excluded. So far, we can only speculate about the real

Table 2. Lateral etch rates across several sampling points of BOE for SiO$_2$ beneath different metal masking stacks of 5 nm Ti covered with 50 nm of Au, Pt, or Cr, respectively and Cr without Ti layer.

BOE etch rate [nm s^{-1}]	Ti/Au pad	Ti/Pt pad	Ti/Cr pad	Cr only pad
Lateral etch rate	12.8 ± 0.3	11.4 ± 0.3	21.5 ± 1.0	14.1 ± 1.0

**ADVANCED
SCIENCE NEWS**

www.advancedsciencenews.com

NANO · MICRO
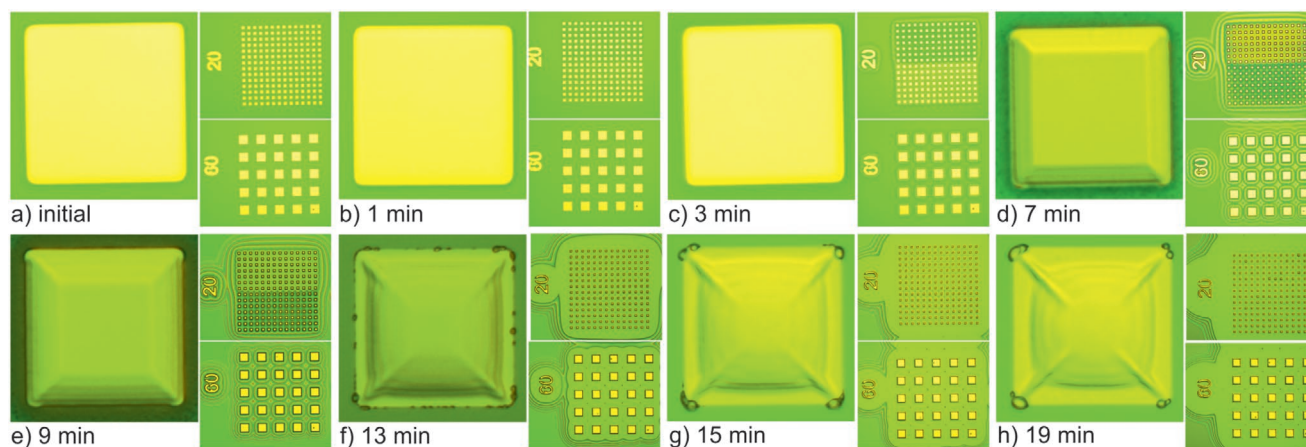
small

www.small-journal.com

Figure 5. a) Vapor-phase HF etching of Au/Ti pads with respect to time. b–e) Clear pyramidal etching is observed for the Au/Ti pad. Once the metal pad reaches the Si interface, f–h) the surface deformation hinders further observance of the real shape (wrinkling visible) (scale bar 20 μm).

origin of the observed effects. Concerning a similar behavior of the pure Cr case, it cannot be excluded that a chromium oxide formed on the thermal silicon oxide–chromium interface during deposition. Chromium is oxygen active forming about 1 nm oxide under ambient conditions and an initial Cr_2O_3 layer during initial physical vapor deposition phase.[28–30] HF does not attack Cr_2O_3 but rather passivates the surface.[31] Thus, a similar interface effect as with the Ti adhesion layer is excluded at the moment. In addition, an isotropic silicon etch with about 5% HF used for a 5 nm Ti/50 nm Au stack on Si did not show any enhanced lateral under etch *despite* the presence of HF and Ti. Similar etch profiles were obtained for fused silica and borofloat wafers (Figure S9, Supporting Information).

Finally, using a polymeric material (SU-8 resist) showed at best only moderate lateral etch rates of 3 nm s^{-1}. In reference experiments, no significant enhancement of lateral etch rates was found for etching of silicon using, for example, 5 nm Ti/50 nm Au films (Figure S10, Supporting Information). Thus, the metal/silicon dioxide interface showed a peculiar behavior. It should be mentioned that perfect SiO_2 pyramidal structures were faithfully transferred into Si by using isotropic silicon etch containing also HF (Figure S11, Supporting Information). This further demonstrates the general behavior and the self-perfecting corner protection mechanism during isotropic etching.

Vapor phase etching is a topic of interest, for example, in advanced X-ray optics.[32] Faceted structures in SiO_2 were obtained in this work for vapor phase HF etching (**Figure 5**). The non-metallized free silicon oxide surface was etched at a constant rate of about 0.14 nm s^{-1} (Figure S3, Supporting Information). This is one order of magnitude smaller than reported in refs. [4] and [26] for vapor phase etching of wet thermal oxide, where water was used as co-solvent (instead of IPA/H_2O) before evaporation and the substrate was at room temperature (instead of 40 °C as in our experiments). The higher substrate temperature in our work reduced the etching rate due to slower HF condensation as well as faster water desorption reaction compared to literature.[4,26,33] HF-vapor etch rates for Au, Pt, and Cr are also reported to be slow or negligible.[22] In comparison to wet etching, the etch rate in the metal-free silicon oxide region is also at least one order

of magnitude smaller. This confirms that vapor-phase etching takes place on metal-free regions. However, a significantly higher etch rate of (1.9 ± 0.2) nm s^{-1} is found for metal-free oxide surfaces *close to but beside* the metal pads (cf. Figure 5e) when compared to reported values for vHF etching and values mentioned before. This is more than ten times faster regarding areas far from metal pads but similar to wet-etch rates in liquid BOE etchant (≈5% HF, cf. Table 1).

The Au/Ti metal pads also clearly showed an enhanced lateral under-etching with a similar pyramidal shape of the SiO_2 body below the pad as observed in the wet etching before. The lateral etch rate under the metal pad in vapor-phase HF etching is about 8.3 nm s^{-1} (Figure S6, Supporting Information). This is well comparable to the unaffected wet silica etching rate using a solution of high concentration of HF of about 50% (cf. Table 1). The Ti/Au metal pad clearly enhances the SiO_2 etching beneath it *as well as* nearby. During the vHF etching of SiO_2 close to the Au pads and the Ti layer below it, a thin capillary starts to form. Such capillaries can give rise to enhanced condensation and reduced evaporation compared to flat surface and bulk situation.[34] With an enhanced condensation, the etching permanently changed to liquid phase etching soon after starting the etch process and resulted in capillary sticking of the metal pad to the oxide surface. From the vapor phase, a continuous supply of reactive species is provided. At oxide surfaces far from the metal films, the reactant water can evaporate thus preventing condensation and remaining in vapor-etch regime, hence, the lower etch rate. From the metal pad, water and dissolved reactive species spread toward surrounding areas. Due to this diffusion-like process, in Figure 5d colored (Newton's) rings are visible indicating a continuous oxide film thickness increase toward the metal-free region further away. The further the liquid spreads away from the pad, the thinner the liquid film gets due to substrate temperature driven evaporation. This region presents a transition from liquid phase to vapor phase etching. The presence of nonvolatile residues along the metal periphery beginning from Figure 5f indicates the presence of a liquid phase below the metal pad allowing diffusion of dissolved species toward the metal pad periphery. Similar to the "coffee stain effect," the evaporation around the metal pad

**ADVANCED
SCIENCE NEWS**
www.advancedsciencenews.com

**NANO · MICRO
small**
www.small-journal.com

drives the observed accumulation at the pad edge (Figure 5e–h). Due to a high effective HF concentration beneath the metal pad and the resulting low selectivity between lateral and vertical etch rate, the vapor-phase process did result in faceted but not in satisfying pyramidal shape (cf. 50% wet etch process for reference).

There was only a slightly preferred water condensation after prolonged storage starting on Au at about (13 ± 0.5) versus (12±0.5) °C for SiO_2 (rel. humidity 40–50%). Wet lift-off processing left traces of undefined organic residues on both SiO_2 and metal. So, condensation behavior is very similar with some preferences for surface perturbations like metal edges.[35–37] This rules out any preferential wetting and supports the explanation by quick formation of wetted capillaries beneath the metal pad. Organic residues might, to a limited extent, reduce the etching rate by surface blocking in vHF etching. In wet etching, however, the non-continuous residue surface will be quickly cleaned and etched.

We demonstrated the fabrication of pyramidal structures in silicon dioxide and glass by utilizing the enhanced lateral under-etching starting from the edges of square metal pads. Obviously, the effective HF concentration determines the selectivity, i.e., the ratio of lateral to vertical etch rate, forming a certain pyramidal slope. Nearly ideal geometries are obtained for low HF concentrations. The wet etching allows for an ideal control of HF concentration, while condensation and evaporation in vapor-phase etching limit the possible control. The under-etching was enabled by an easily etched interface between the metal pad (Pt, Au, or Cr) and the silicon dioxide surface. However, this was not only due to the fast etching titanium adhesion layer. It was of much more general behavior originating from disturbed interfaces. The finally obtained pyramidal structures are perfect in shape and can be used for surface texturing in photovoltaics or light-emitting diodes as well as for the direct fabrication of dedicated atomic force microscopy tips in SiO_2. The latter becomes possible by combining high aspect ratio dry etch processes with the here presented wet etch for post-processing and sharpening. Additional applications are plasmonic structures. The intrinsically low vertical etch rate limits all geometries to rather shallow ones unless one succeeds in enhancing it but without influencing the lateral etch rate. We see strong potential to influence the ratio of lateral/vertical etch rates by modifying the metal deposition parameters enabling a higher diversity of interesting applications.

Experimental Section

All used chemical were of VLSI grade.

Metal Patterning: Silicon ⟨100⟩ substrates with 1 µm wet oxide were pre-tempered at 120 °C for 2 min and adhesion promoter coated with hexadimethylsilazane (HMDS) in a customized vapor coating system for 5 min. Photoresist 5114E (vendor) was spin-coated on prepared substrates with about 900 nm film thickness, soft-baked at 75 °C for 3 min and at 110 °C for 3 min and finally exposed in an optical mask aligner system (EVG 6200, EV Group, Austria). The resist was developed in a puddle development system (Convac). By electron beam evaporation (MS150x4-AE-B, FHR Anlagenbau GmbH, Germany), a titanium adhesion promoter was deposited along with gold, platinum, or chromium layers. Prior to the metal deposition, an Ar sputter cleaning was used (RF power 100 W, 1 min, bias voltage 650 V, base pressure 2e-7 mbar). 5 nm Ti was evaporated at a rate of 0.2 nm s⁻¹, (0.8–1e-7 mbar). The rate for 50 nm Au was 0.5 nm s⁻¹ (0.8–2e-7 mbar). Finally, the sample was immersed in propane-2-on (acetone) and ultrasound agitation (Sonorex, BANDELIN electronic GmbH & Co. KG) was used to initiate the lift-off. Samples were cleaned in acetone, 2-propanol and clean water (DIN ISO 3696; <0.1 µS cm⁻¹).

Substrates: Thermal oxide (wet oxidation, 1 µm thick), borofloat (BF33 Schott), silicon wafer (Si 100), fused silica.

Wet HF Etching: The buffered oxide etch solution (BOE) was prepared using 1064 mL 42% ammonium fluoride (NH_4F), 682 mL acetic acid, 193 mL 50% hydrofluoric acid (HF), and 61 mL clean water to get 5% BOE solution. Unbuffered 5% HF was diluted with clean water from commercial 50% HF etching solution (Honeywell); 50% HF was used as delivered. Etching was done using manual dip into the etchant with subsequent clean water rinse to stop the etching process. Finally, samples were blow-dried with N_2.

Vapor-Phase HF Etching: The samples were placed in a commercial gas phase etcher (HF Vapor Phase Etcher, Idonus Sarl) and electrostatically chucked with a chuck temperature of 40 °C. The reaction chamber was filled with a mixture of 80 mL 50% aqueous HF and 20 mL 2-propanol. After time steps of 1 or 2 min, the samples were removed and inspected. On the whole sample surface, macroscopic liquid droplets became visible after continuous etching of 2 min. The measurements on the free silicon surface were done in a significant distance to the mold patterns (about 3 mm distance) using white light reflectometry (FTP advanced, Sentech).

Isotropic Si Etch: Isotropic silicon etchant was prepared from 10 mL 50% HF, 30 mL 100% acetic acid, and 60 mL 65% nitric acid giving effectively 5% HF solution.

Measurements Under-Etch: Measured of the lateral under-etch distance was obtained from multiple optical microscopy images using ImageJ to calculate mean and standard deviation (given as mean ± standard deviation).

Supporting Information

Supporting Information is available from the Wiley Online Library or from the author.

Acknowledgements

Conflict of Interest

The authors declare no conflict of interest.

Keywords

[1] P. Pal, K. Sato, *Micro Nano Syst. Lett.* **2015**, *3*, 6.
[2] H. Seidel, L. Csepregi, A. Heuberger, H. Baumgärtel, *J. Electrochem. Soc.* **1990**, *137*, 3612.
[3] E. J. W. Berenschot, H. V. Jansen, N. R. Tas, *J. Micromech. Microeng.* **2013**, *23*, 055024.
[4] A. Boisen, J. P. Rasmussen, O. Hansen, S. Bouwstra, *Microelectron. Eng.* **1996**, *30*, 579.
[5] Y. Wang, L. Yang, Y. Liu, Z. Mei, W. Chen, J. Li, H. Liang, A. Kuznetsov, D. Xiaolong, *Sci. Rep.* **2015**, *5*, 10843.
[6] H. Schumacher, U. Künzelmann, B. Vasilev, K.-J. Eichhorn, J. W. Bartha, *Appl. Spectroscop.* **2010**, *64*, 1022.
[7] K. P. Rola, *Microsyst. Technol.* **2017**, *23*, 1463.
[8] M. Nagai, K. Nakanishi, H. Takahashi, H. Kato, T. Makino, S. Yamasaki, T. Matsumoto, T. Inokuma, N. Tokuda, *Sci. Rep.* **2018**, *8*, 6687.
[9] P. Hou, R. Kumar, B. Oberleiter, R. Kohns, D. Enke, U. Beginn, H. Fuchs, M. Hirtz, M. Steinhart, *Adv. Funct. Mater.* **2020**, *30*, 2001531.
[10] B. Ai, Y. Yu, H. Möhwald, L. Wang, G. Zhang, *ACS Nano* **2014**, *8*, 1566.
[11] Y. H. Kim, J. Lee, W. M. Kim, C. Fuchs, S. Hofmann, H.-W. Chang, M. C. Gather, L. Müller-Meskamp, K. Leo, *Adv. Funct. Mater.* **2014**, *24*, 2553.
[12] X. Wu, W. Sun, L. Sun, K. Guo, M. Tang, P. Zhou, *Org. Electron.* **2014**, *15*, 3615.
[13] P. C. Simpson, A. T. Woolley, R. A. Mathies, *Biomed. Microdevices* **1998**, *1*, 7.
[14] R. Kometani, T. Murakami, E. Maeda, presented at 29th Int. Micropr. and Nanotech. Conf. (MNC), Kyoto (Japan), **2016**, 11.
[15] R. Kometani, T. Murakami, E. Maeda, presented at 42nd Int. Conf. Micro Nano Engineering (MNE), Vienna (Austria), **2016**, 9.
[16] R. Kometani, M. Okuno, S. Warisawa, presented at 62nd Int. Conf. Electron, Ion Photon Beam Techn. Nanofab. (EIPBN), Puerto Rico, **2018**, 5.
[17] N. Pekas, Q. Zhang, M. Nannini, D. Juncker, *Lab Chip* **2010**, *10*, 494.
[18] R. Kirchner, V. A. Guzenko, H. Schift, *Adv. Opt. Technol.* **2019**, *8*, 175.
[19] R. Fallica, R. Kirchner, H. Schift, Y. Ekinci, *Microelectron. Eng.* **2017**, *177*, 1.
[20] C. M. Waits, A. M. Modafe, R. Ghodssiu, *J. Micromech. Microeng.* **2013**, *12*, 170.
[21] I. Khazi, U. Mescheder, U. Muthiah, *Microelectron. Eng.* **2018**, *193*, 34.
[22] Z. Huang, N. Geyer, P. Werner, J. de Boor, U. Gösele, *Adv. Mater.* **2011**, *23*, 285.
[23] D. J. Monk, D. S. Soane, R. T. Howe, *Thin Solid Films* **1993**, *232*, 1.
[24] E. Klokholm, B. S. Berry, *J. Electrochem. Soc.* **1968**, *115*, 823.
[25] C. R. Helms, B. E. Deal, *J. Vac. Sci. Technol., A* **1992**, *10*, 806.
[26] K. R. Williams, K. Gupta, M. Wasilik, *J. Microelectromech. Syst.* **2003**, *12*, 761.
[27] B.-P. Zhang, H. Habazaki, A. Kawashima, K. Asami, K. Hashimoto, *Corros. Sci.* **1993**, *34*, 599.
[28] F. Watari, *Surf. Sci.* **1981**, *110*, 111.
[29] J. Vancea, G. Reiss, F. Schneider, K. Bauer, H. Hoffmann, *Surf. Sci.* **1989**, *218*, 108.
[30] T. Jukna, J. Baltrušaitis, V. Sinkevičius, D. Viržonis, *Thin Solid Films* **2008**, *516*, 2943.
[31] S. Brunet, B. Requieme, E. Colnay, J. Barrault, M. Blanchard, *Appl. Catal., B* **1995**, *5*, 305.
[32] L. Romano, M. Kagias, J. Vila-Comamala, K. Jefimovs, L. T. Tseng, V. A. Guzenko, M. Stampanoni, *Nanoscale Horiz.* **2020**, *5*, 869.
[33] C. R. Helms, B. E. Deal, *J. Vac. Sci. Technol., A* **1992**, *10*, 806.
[34] N. Maeda, J. N. Israelachvili, M. M. Kohonen, *Proc. Natl. Acad. Sci. USA* **2003**, *100*, 803.
[35] J. L. McCormick, E. Baer, *Dropwise Condensation on Horizontal Surfaces*, Department of Chemistry and Chemical Engineering, University of Illinois, **1962**.
[36] J. L. McCormick, E. Baer, *J. Colloid Sci.* **1963**, *18*, 208.
[37] A. Ashrafi, A. Moosavi, *J. Appl. Phys.* **2016**, *120*, 124901.
[38] R. Dewan, I. Vasilev, V. Jovanov, D. Knipp, *J. Appl. Phys.* **2011**, *110*, 013101.